Numerical Investigation of Chip Cooling Using Volume Averaging Technique (VAT)

A. Horvat [1], M. Rizzi [2], I. Catton [3]

[1] *"Jožef Stefan" Institute, Reactor Engineering Division*
Jamova 39, SI-1000 Ljubljana, Slovenia

[2,3] *Morrin-Martinelli-Gier Memorial Heat Transfer Laboratory*
Department of Mechanical and Aerospace Engineering
School of Engineering and Applied science
University of California, Los Angeles

Abstract

The present paper describes construction of an algorithm for conjugate heat transfer calculations in order to find the most suitable form for a heat sink. Applying Volume Averaging Theory (VAT) to a system of transport equations, a heat exchanger structure was modeled as a homogeneous porous media. The example numerical simulations were performed for test sections with isothermal structure as well as with heat conducting Al pin-fins. The geometry of the simulation domain and boundary conditions followed the geometry of the experimental test section used in the Morrin-Martinelli-Gier Memorial Heat Transfer Laboratory at University of California, Los Angeles. The comparison of the drag coefficient C_d as a function of Reynolds number Re_h reveals good agreement with already published data, whereas the comparison of the Nusselt number distributions shows much larger discrepancies. Finite conductivity of a solid phase decreases the heat transfer coefficient and the Nusselt number. The influence of conductivity becomes larger with increasing Reynolds number.

1 Introduction

Heat exchangers are one of the basic installations not only in power and process industries, but also in electronic equipment production. Despite their crucial role, there is still a great deal of empiricism involved in the design procedure of heat exchangers. Namely, the development and application of heat exchangers and their surfaces has taken place in a piecemeal fashion in a number

of rather unrelated areas, principally those of the automotive and prime mover, aerospace, cryogenic and refrigeration sectors. Much detailed technology, familiar in one sector, progressed only slowly over the boundary into another sector [1]. Therefore, the unifying approach to select and to optimise the heat exchanger design can bring significant cost reduction to industry.

The present paper is a part of a broader effort to develop a scientific procedure for optimization of heat exchanger geometries. It describes construction of an algorithm for conjugate heat transfer calculations in order to find the most suitable form for a heat sink. Applying Volume Averaging Theory (VAT) (see [2-4] for details) to a system of transport equations, a heat exchanger structure was modeled as a homogeneous porous media. The interaction between fluid and heat sink structure, the VAT equation closure requirement, was accomplished with drag and heat transfer coefficients, which were taken from the available literature and inserted into a computer code.

The example numerical simulations were performed for test sections with isothermal structure as well as with heat conducting Al pin-fins. In both cases the pin-fins had staggered arrangement with a pitch-to-diameter ratio of p/d = 1.5. The Reynolds number, based on hydraulic diameter, spanned from Re_h = 167 to Re_h = 1964. The calculated whole-section drag coefficient, thermal effectiveness and Nusselt number were compared with available experimental data [5]. The comparison shows a reasonable good agreement with experimental data despite model simplifications.

2 Model

The airflow through a chip cooler structure can be described with basic mass, momentum and heat transport equations [6]. Due to requirement for the model to have short computing times, the transport equations have to be averaged over a periodic control volume (see [4] for details). This volumetric averaging technique (VAT) leads to a closure problem, where interface exchange of momentum and heat between fluid and solid phase have to be described with additional empirical relations e.g. a local drag coefficient C_d and a local heat transfer coefficient h.

To further simplify the simulated system, fluid flow was taken as unidirectional with a constant pressure drop. As a consequence, the velocity changes only transverse to the flow direction. This means that the streamwise pressure gradient across the entire simulation domain is balanced with shear stresses. Thus the momentum equation can be written in differential form as:

$$-\alpha_f \hat{\mu}_f \left(\frac{\partial^2 \hat{u}_f}{\partial \hat{y}^2} + \frac{\partial^2 \hat{u}_f}{\partial \hat{z}^2} \right) + \frac{1}{2} C_d \hat{\rho}_f \hat{u}_f^2 \hat{S} = \frac{\Delta \hat{p}}{\hat{\ell}_x} \tag{1}$$

where α_f is a fluid phase fraction, C_d a local drag coefficient, S a specific surface of porous media, Δp a pressure drop across simulation domain and ℓ_x a simulation domain length.

The temperature field in fluid phase is formed as a balance between thermal convection in the streamwise direction, thermal diffusion and heat, which is transferred from solid phase to fluid. Thus the differential form of energy equation for fluid phase is:

$$\alpha_f \hat{\rho}_f \hat{c}_f \hat{u}_f \frac{\partial \hat{T}_f}{\partial \hat{x}} = \alpha_f \hat{\lambda}_f \left(\frac{\partial^2 \hat{T}_f}{\partial \hat{x}^2} + \frac{\partial^2 \hat{T}_f}{\partial \hat{y}^2} + \frac{\partial^2 \hat{T}_f}{\partial \hat{z}^2} \right) - \hat{h}\left(\hat{T}_f - \hat{T}_s\right)\hat{S} \tag{2}$$

where T_f is the fluid phase and T_s is the solid phase temperature. The heat transfer between solid and fluid phase is modelled as a linear relation between both phase temperatures, where h is a local heat transfer coefficient.

The chip cooler structure in each control volume is only loosely connected in horizontal directions. As a consequence, only the thermal diffusion in vertical direction is in balance with heat leaving the structure through a fluid-solid interface, whereas the thermal diffusion in horizontal directions can be neglected. This simplifies energy equation for solid phase to:

$$0 = \alpha_s \hat{\lambda}_s \frac{\partial^2 \hat{T}_s}{\partial \hat{z}^2} + \hat{h}\left(\hat{T}_f - \hat{T}_s\right)\hat{S} \tag{3}$$

where α_s is a solid phase fraction.

The eqs. (1-3), written with phase averaged variables, are equations for steady-state transport of momentum and heat through homogeneous porous media. The reliable empirical data for two additional parameters, a local drag coefficient C_d and a local heat transfer coefficient h, were found in [7-9].

3 Simulation domain

The geometry of the simulation domain as well as boundary conditions for eqs. (1-3) follow the geometry of experimental test section used in the Morrin-Martinelli-Gier Memorial Heat Transfer Laboratory at University of California, Los Angeles, where experimental data described in [5] were taken.

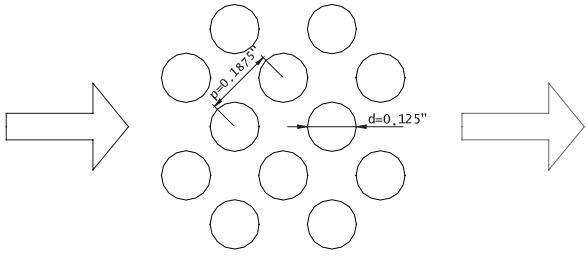

Figure 1: Pin-fins arrangement in the simulated case.

3.1 Geometry

The general arrangement of pin-fins in the simulation domain is given in Fig. 1. The diameter of pin-fins was d = 0.003175 m (0.125"). The pitch-to-diameter ratio in streamwise direction was set to p_x/d = 1.06 and in transverse direction to p_y/d = 2.12. The simulation domain consisted of 34 rows of pin-fins in streamwise direction and 17 rows of pin-fins in transverse direction.

3.2 Boundary conditions

The no-slip boundary conditions for the momentum equation (1) were implemented for all 4 walls parallel with the flow direction:

$$\hat{u}_f(0,\hat{z}) = 0\,, \quad \hat{u}_f\left(\hat{L}_y,\hat{z}\right) = 0\,, \quad \hat{u}_f(\hat{y},0) = 0\,, \quad \hat{u}_f\left(\hat{y},\hat{L}_z\right) = 0 \tag{4}$$

As a flow driving force, the whole-section pressure drop Δp was prescribed. The absolute values are summarised in Table 1.

For the fluid phase energy equation (2), the simulation domain inflow and the bottom wall were taken as isothermal:

$$\hat{T}_f(0,\hat{y},\hat{z}) = \hat{T}_{in}\,, \quad \hat{T}_f(\hat{x},\hat{y},0) = \hat{T}_{if} \tag{5}$$

whereas the rest of walls were considered as adiabatic:

$$\begin{aligned} &\frac{\partial \hat{T}_f}{\partial \hat{x}}\left(\hat{L}_x,\hat{y},\hat{z}\right) = 0\,, \quad \frac{\partial \hat{T}_f}{\partial \hat{y}}(\hat{x},0,\hat{z}) = 0\,, \\ &\frac{\partial \hat{T}_f}{\partial \hat{y}}\left(\hat{x},\hat{L}_y,\hat{z}\right) = 0\,, \quad \frac{\partial \hat{T}_f}{\partial \hat{z}}\left(\hat{x},\hat{y},\hat{L}_z\right) = 0 \end{aligned} \tag{6}$$

For the solid phase energy equation (3), the bottom wall was prescribed as isothermal, whereas the top wall was assumed to be adiabatic:

$$\hat{T}_s(\hat{x},\hat{y},0) = \hat{T}_{if}\,, \quad \frac{\partial \hat{T}_s}{\partial \hat{z}}\left(\hat{x},\hat{y},\hat{L}_z\right) = 0 \tag{7}$$

The assumption about the isothermal bottom wall (5, 7) significantly differs from the experimental set-up [5], where the pin-fins were connected with a conductive base plate. Nevertheless, as the results will show, the presented model still give a satisfactory approximation of the measured values.

The absolute temperatures in different simulation cases are summarised in Table 1.

Table 1: Boundary conditions - pre-set values.

No.	Δp[Pa]	T_{In} [°C]	T_{If} [°C]
1	5.00	22.20	35.00
2	6.00	22.20	35.00
3	8.00	22.20	35.00
4	10.00	22.20	35.00
5	30.00	22.20	35.00

No.	Δp[Pa]	T_{In} [°C]	T_{If} [°C]
6	50.00	22.20	35.00
7	74.65	22.72	34.30
8	180.4	22.95	31.56
9	279.9	22.20	30.30
10	385.7	22.23	29.88

4 Numerical methods

The transport equations (1-3) and boundary equations (4-7) were transformed into the dimensionless form and then discretized following principles of the finite volume methods [6, 10]. Due to boundary conditions (5-7), the velocity v_x as well as the solid phase temperature T_s were described as two-dimensional scalar fields, whereas the fluid phase temperature T_f as a three-dimensional scalar field. This resulted in a non-symmetric five diagonal matrix system for two-dimensional scalar fields and a seven diagonal matrix system for three-dimensional scalar fields.

In order to invert the matrix systems efficiently, a preconditioned conjugate gradient method, described in [11], was adopted for this specific problem.

5 Results and discussion

The results of an example calculation are presented in Figs. 2 and 3. The imposed pressure drop Δp = 180.4 Pa causes airflow of Reynolds number Re_h = 1295.12, where the definition of the Reynolds number is based on hydraulic diameter d_h of hypothetical porous media channel:

$$Re_h = \frac{\bar{\hat{u}}}{\hat{\nu}_f}\hat{d}_h = \frac{\bar{\hat{u}}}{\hat{\nu}_f}\left(4\frac{\hat{\Omega}_f}{\hat{S}_{f\to s}}\right) \tag{8}$$

Ω_f marks a fluid phase volume and $S_{f\to s}$ a solid-fluid interface area.

Fig. 2 shows the temperature field in Al structure, whereas the temperature field in airflow is revealed in Fig. 3.

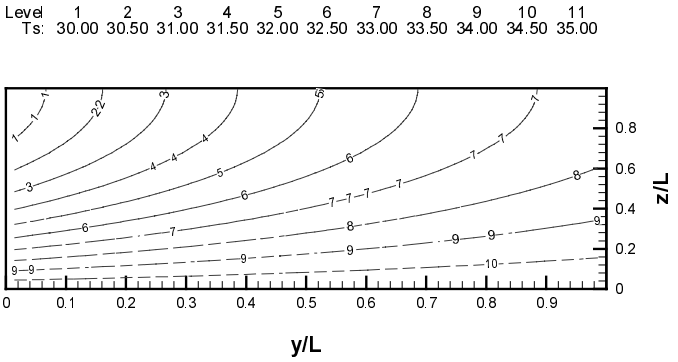

Figure 2: Temperature fields in solid at Re_h = 1295.12, T_{In} = 22.2 °C, T_B = 35 °C

The temperatures are presented with isotherms. In Fig. 2, the Al structure has its highest temperature close to the isothermal bottom and the lowest close to the upper edge, where the structure is exposed to the low-temperature inflow. Fig. 3 shows how air is gradually heated from the inlet on the left side to the outlet on the right side. The lower part of the temperature field also shows the intensive heating from the isothermal bottom boundary, which results in horizontal thermal stratification of passing air.

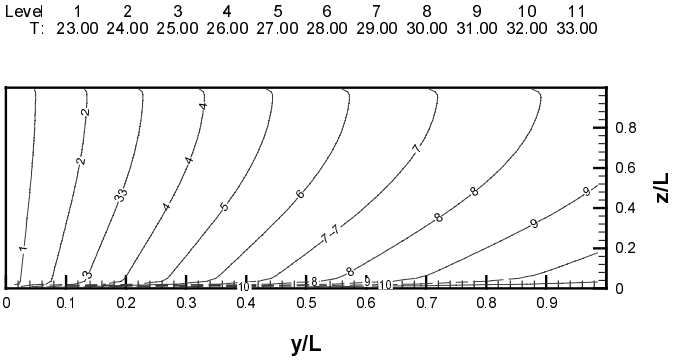

Figure 3: Temperature fields in air at Re_h = 1295.12, T_{In} = 22.2 °C, T_B = 35 °C.

Beside the example calculation, two other series of calculations with 10 different pressure drops were performed. Boundary conditions for these calculations are summarised in Table 1. In both series, the Al material properties were taken for the heat sink and air material properties for coolant flow. Nevertheless, the first series of calculations were made with infinite thermal conductivity to inspect the influence of thermal conductivity.

As it is usually the case in such calculations, the whole-section drag coefficient C_d (9) and Nusselt number Nu (10) were calculated and compared with experimental results [5].

$$\overline{C}_d = \frac{2\Delta\hat{p}}{\hat{\rho}_f \overline{\hat{u}}^2 \hat{\ell}_x \hat{S}} \tag{9}$$

$$\overline{Nu} = \frac{\hat{\dot{Q}}\hat{d}_h}{\Delta\hat{T}\hat{A}_{base}\hat{\lambda}_f} \tag{10}$$

In the Nusselt number (10) definition, the convective heat transfer rate is defined as

$$\hat{\dot{Q}} = \alpha_f \hat{\rho}\hat{c}_p \left(\hat{T}_{out} - \hat{T}_{in}\right)\hat{A} \tag{11}$$

whereas $\Delta\hat{T}$ is a temperature difference between a heated bottom and inflow air.

The comparison on Fig. 4 shows the whole-section drag coefficient C_d (9) as a function of Reynolds number Re_h (8). It reveals good agreement with already published data. Nevertheless, at higher Reynolds number the difference of few percents appears due to increasing turbulence, which was not taken into account in the model.

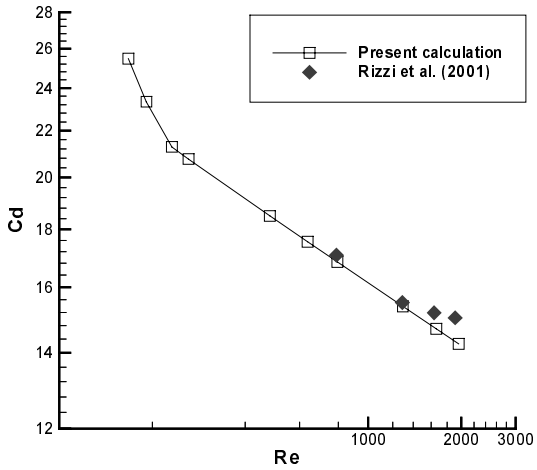

Figure 4: Reynolds number Re_h dependence of drag factor C_d.

The comparison of the Nusselt number distributions in Fig. 5 shows much larger discrepancies. Due to the difference in thermal boundary conditions, the calculated data reveal up to 45 percent higher heat transfer rate than the measured values. Furthermore, the calculated data reveals that finite conductivity

of the Al structure (marked with Al) decreases heat transfer coefficient and Nusselt number. The influence of finite conductivity of the solid phase becomes larger with increasing Reynolds number.

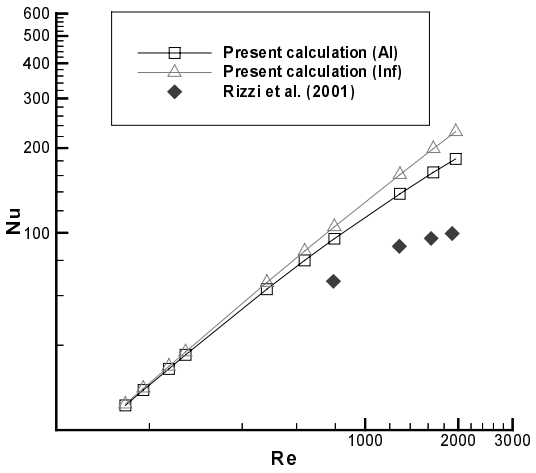

Figure 5: Reynolds number Re_h dependence of Nusselt number Nu.

The design of a heat exchanger involves consideration of both the heat transfer rates and the mechanical pumping power expended to overcome fluid friction and move the fluid through the structure. Thus the main design goal is to maximise the heat transfer rate (11) at minimum pumping power:

$$\hat{\dot{W}} = \alpha_f \, \Delta\hat{p} \, \hat{A}_\perp \, \bar{\hat{u}} \tag{12}$$

Fig. 6 shows the effectiveness of the heat transfer process defined as ratio between the heat transfer rate (11) and the mechanical power (12) spent to overcome the fluid-structure friction. The experimental as well as numerical results are close together. At decreasing effectiveness, the influence of solid structure finite thermal conductivity increases and reaches 15 percent at Reynolds number $Re_h \approx 2000$.

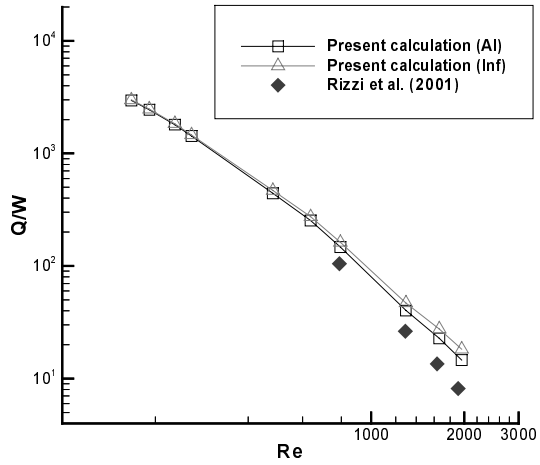

Figure 6: Reynolds number Re_h dependence of heat sink effectiveness Q/W .

As it is presented, the thermal effectiveness of the examined heat sink reduces with increasing Reynolds number. Although, the lower Reynolds numbers bring higher effectiveness, resulting low heat transfer rates have to be compensated with a larger heat transfer surface and consequently with a larger size of the heat exchanger. In some cases this is not possible due to economics and size limitations.

6 Conclusions

The present paper describes an effort to develop a fast running numerical algorithm for heat exchanger calculations. The purpose of the task was to numerically investigate heat removal from an electronic chip. The heat sink internal structure, in form of a staggered arrangement of pin-fins, was treated as a homogenous porous media. The local values of drag and heat transfer coefficients that were needed to close the transport equations were taken from [7-9]. The resulting partial differential equations were discretized using the momentum and energy conservation properties of the finite volume method. The resulting system of semilinear equations was solved with a preconditioned conjugate gradient method. To test the calculation procedure an experimental test section that has been used in the Morrin-Martinelli-Gier Memorial Heat Transfer Laboratory was selected.

Two series of calculations were performed for the Al heat sink cooled with airflow. The calculated values of the whole-section drag coefficient show good agreement with published data, whereas the calculated values of the Nusselt number reveal large discrepancies due to differences in thermal boundary conditions. Also the influence of finite thermal conductivity of the solid structure

was examined. It was shown that finite thermal conductivity of Al decreases thermal effectiveness for 15 percent at Re_h = 2000. Furthermore, it is expected that at higher Reynolds number, this conductivity effect would increase.

The present results demonstrate that the selected approach is appropriate for heat exchanger calculations were a thermal conductivity of a solid phase has to be taken into account. The example calculations also verify that the developed numerical code yields sufficiently accurate results to be applicable also elsewhere.

Acknowledgements

The first author's financial support by the Kerze-Cheyovich scholarship is gratefully acknowledged.

References

[1] Hesselgreaves, J.E., *Compact Heat Exchangers Selection, Design and Operation*. Pergamon Press, 2001.

[2] Whitaker, S., Diffusion and Dispersion in Porous Media. *AIChE Journal*, Vol. 13, No. 3, pp. 420-427, 1967.

[3] Travkin, V.S., & Catton, I., A Two Temperature Model for Fluid Flow and Heat Transfer in a Porous Layer. *J. Fluid Engineering*, Vol. 117, pp. 181-188, 1995.

[4] Travkin, V.S., & Catton, I., Transport Phenomena in Heterogeneous Media Based on Volume Averaging Theory. *Advans. Heat Trasfer*, Vol. 34, pp. 1-143, 1999.

[5] Rizzi, M., Canino, M., Hu, K., Jones, S., Travkin, V., Catton, I., Experimental Investigation of Pin Fin Heat Sink Effectiveness. *Proc. of the 35th National Heat Transfer Conference*, Anaheim, California, 2001.

[6] Horvat, A., Catton, I., Development of an Integral Computer Code for Simulation of Heat Exchangers. *Proc. of the Conf. "Nuclear Energy in Central Europe 2001"*, Portorož, Slovenia, Sept. 10-13, 2001, No. 213, 2001.

[7] Launder, B.E., Massey, T.H., The Numerical Prediction of Viscous Flow and Heat Transfer in Tube Bank. *Trans. ASME J. Heat Transfer*, Vol. 100, pp. 565-571, 1978.

[8] Kays, W.M., London, A.L., *Compact Heat Exchangers*. 3rd Ed. Krieger Publishing Company: Malabar, Florida, pp. 146-147, 1998.

[9] Žukauskas, A.A., Ulinskas, R., Efficiency Parameters for Heat Transfer in Tube Banks. *J. Heat Transfer Engineering*, Vol.5, No.1, pp. 19-25, 1985.

[10] Versteeg, H.K. & Malalasekera, W., *An Introduction to Computational Fluid Dynamics, The Finite Volume Method*, Longman Scientific & Technical: England, pp. 103-133, 1995.

[11] Ferziger, J.H., Perić, M., *Computational Method for Fluid Mechanics, Chapter 5: Solution of Linear Equation Systems*. Springer Verlag: Berlin, pp. 85-127, 1996.